Available online at www.sciencedirect.com
ScienceDirect
International Journal of Heat and Mass Transfer 50 (2007) 3195–3202
International Journal of HEAT and MASS TRANSFER
www.elsevier.com/locate/ijhmt

Influence of capillary forces on water injection into hot rock, saturated with superheated vapour

G.G. Tsypkin [a], C. Calore [b,*]

[a] Institute for Problems in Mechanics, RAS, Vernadskogo Ave. 101, 119420 Moscow, Russia
[b] Istituto di Geoscienze e Georisorse – CNR, Sezione di Firenze, via La Pira 4, 50121 Florence, Italy

Received 7 December 2005
Available online 27 February 2007

Abstract

The results of a theoretical study and numerical analysis of the role of capillary pressure of cold water injection into depleted geothermal reservoirs are presented. A simplified 1-D mathematical model is developed, that describes the motion of a sharp vaporization front. Some asymptotic estimates for a wide range of parameters are given and a similarity solution is derived. Analytical results are then compared with those obtained from the numerical reservoir simulator TOUGH2, showing a good agreement between the two.

Keywords: Water injection; Capillary pressure; Analytical solution; Numerical simulation

1. Introduction

The influence of capillary forces on fluid flow in porous media has been the subject of numerous theoretical and experimental studies over the past decade. The aim of the present study was to develop a mathematical model for a better understanding of the physical processes occurring in geothermal systems. One of the most important processes in geothermal reservoirs under exploitation and/or recharge is capillarity, as it has a substantial influence on fluid phase changes. The effects of capillarity on phase changes are also of significance to Hot Dry Rock technology. Capillary pressure effects in porous rocks were studied, among others, by Udell [1], Pruess and O'Sullivan [2], Pruess [3] and Li and Horne [4,5]. Pruess and O'Sullivan [2] reported the numerical simulations that were performed to evaluate the impact of capillarity and vapour adsorption on the depletion of vapour-dominated geothermal reservoirs.

The numerical simulator TOUGH2 [6] for multiphase heat and fluid flow represents a powerful tool for modelling a large part of the wide spectrum of physical phenomena occurring in geothermal reservoirs. However the treatment of simpler physical situations, for which solutions exist in a closed analytical form, is a necessary step towards our understanding of the essential features of the phenomena involved. Analytical solutions can, moreover, also prove the behavior and accuracy of complex numerical simulators.

Frontal solutions play a fundamental role in the theoretical investigation of phase transition problems. These solutions imply that phase transition takes place over a narrow region or sharp front that can be considered as a discontinuity of the water saturation function, and that this interface separates single-phase zones. This method has been applied to geothermal reservoir modelling, as in, for example, Udell [1], Pruess et al. [7], Garg and Pritchett [8], Woods and Fitzgerald [9], Barmin and Tsypkin [10], Woods [11] and Tsypkin and Woods [12]. As a rule, the frontal formulation admits the derivation of an explicit solution in some specific cases, and numerical methods are usually verified by comparing their results with analytical solutions. Traditionally, derivation of the exact and explicit solution is the first step in a new mathematical model, providing insight into physical processes. Recently,

* Corresponding author. Tel.: +39 055 2757668; fax: +39 055 290312.
E-mail address: calore@igg.cnr.it (C. Calore).

0017-9310/$ - see front matter © 2007 Elsevier Ltd. All rights reserved.
doi:10.1016/j.ijheatmasstransfer.2006.12.010

Nomenclature

a	thermal diffusivity [m^2/s]
C	specific heat [J/(K kg)]
C_p	specific heat of vapour at constant pressure [J/(K kg)]
d	typical length scale of a pore [m]
k	permeability [m^2]
L	length scale [m]
P	pressure [Pa]
P_c	capillary pressure [Pa]
P_f	pressure at the flat surface [Pa]
q	specific heat of vaporization [J/kg]
R	gas constant [J/(kg K)]
R_0	universal gas constant [J/(mol K)]
r	mean radius of the capillary meniscus [m]
t	time [s]
T	temperature [K]
V	velocity of the vaporization front [m/s]
V_m	molar volume of water [m^3/mol]
$\mathbf{v}$	filter velocity [m/s]
x	coordinate [m]
$X(t)$	position of the vaporization front [m]

Greek symbols

α_w	water compressibility coefficient [1/Pa]
Δ	Laplace operator
γ	dimensionless similarity coordinate of the vaporization front
κ	conductivity coefficient [m^2/s]
θ	contact angle [degree]
λ	thermal conductivity [W/(m K)]
μ	viscosity [Pa s]
ρ	density [kg/m^3]
σ	surface tension [J/m^2]
ϕ	porosity
ζ	dimensionless similarity variable

Subscripts

n	normal
0	initial value
s	porous medium skeleton
v	vapour
w	water
+	quantities to the right of the front
−	quantities to the left of the front
*	values of the quantities at the front
1	vapour domain
2	water domain

Superscript

0	boundary value

we applied this analytical approach to the problem of vapour extraction from water-saturated geothermal reservoirs [13,14].

In the present paper we extend our analysis to the problem of cold water injection into hot rock saturated with superheated vapour, assuming that a sharp vaporization front separates the water- and vapour-saturated zones. This is a typical case in which the effects of capillarity on heat and mass transfer processes in porous rocks play a very important role.

The paper is organized as follows. In Section 2, a mathematical model of cold water injection into vapour-saturated hot rock is developed. The injection process leads to formation of the sharp liquid front that separates the water-saturated and vapour-saturated regions. A full system of boundary conditions at the interface, which takes into account capillary forces, is then derived. In Section 3, the problem is reduced to a system of transcendental equations by a similarity solution approach. Using asymptotic estimates and numerical modelling with TOUGH2, the influence of capillary forces on the boiling process induced by cold water injection is investigated. In Section 4 we compare the results of the analytical model and numerical simulations, confirming that two different boiling regime exist: (1) with formation of a two-phase transition zone and (2) with formation of a sharp vaporization front. The conclusions are given in Section 5.

2. Problem formulation

Consider the injection of pure cold water into a high-temperature geothermal reservoir saturated with superheated vapour. If the porous rock is initially superheated then, as the injected liquid vaporizes, a boiling front develops, producing vapour ahead of the front. In order to describe the dynamics and thermodynamics of liquid and vapour flow through the porous rock we use Darcy's law, mass and energy conservation laws, and the equation of state for water and vapour (see, for example, [15,16]). Being the movement of water and vapour through porous media usually slow, fluid and rock are assumed to be in local thermodynamic equilibrium, owing to thermal diffusion between the solid and fluid [16].

2.1. Basic equations

In the vapour region, combining the equations for vapour flow according to the above assumptions and laws, the following system of two equations for the temperature and pressure is obtained [14]:

$$\frac{\partial P_v}{\partial t} - \frac{P_v}{T}\frac{\partial T}{\partial t} - \frac{k}{\phi\mu_v}(\operatorname{grad} P_v)^2 = -\frac{k}{\phi\mu_v}\frac{P_v}{T}\operatorname{grad} P_v \operatorname{grad} T + \frac{k}{\phi\mu_v}P_v\Delta P_v \quad (1)$$

$$(\rho C)_1 \frac{\partial T}{\partial t} - \frac{k}{\mu_v}\rho_v C_p \operatorname{grad} P_v \operatorname{grad} T = \operatorname{div}(\lambda_1 \operatorname{grad} T)$$
$$\lambda_1 = \phi\lambda_v + (1-\phi)\lambda_s, \quad (\rho C)_1 = \phi\rho_v C_v + (1-\phi)\rho_s C_s \quad (2)$$

Analogously, a system of two equations for the temperature and pressure is obtained for the water region. If pressure is sufficiently less than $1/\alpha_w$, then the mass conservation equation can be simplified to the linear form

$$\frac{\partial P_w}{\partial t} = \kappa \Delta P_w \quad \text{where } \kappa = \frac{k}{\phi \alpha_w \mu_w} \quad (3)$$

and the energy equation takes the form

$$(\rho C)_2 \frac{\partial T}{\partial t} - \frac{k}{\mu_w}\rho_w C_w \operatorname{grad} P_w \operatorname{grad} T = \operatorname{div}(\lambda_2 \operatorname{grad} T)$$
$$\lambda_2 = \phi\lambda_w + (1-\phi)\lambda_s, \quad (\rho C)_2 = \phi\rho_w C_w + (1-\phi)\rho_s C_s \quad (4)$$

2.2. Boundary conditions

We assume that vaporization occurs at the sharp front that migrates outwards from the injection well. The boundary conditions across the front may be obtained from the conservation of mass and energy, assuming that water and vapour are in local thermodynamic equilibrium. These relations are supplemented by the Clausius–Clapeyron equation which determines the boiling pressure as a function of boiling temperature. Conservation of mass and energy through the interface takes the form

$$\phi\left(1 - \frac{\rho_v}{\rho_w}\right) V_n = \frac{k}{\mu_v}\frac{\rho_v}{\rho_w}(\operatorname{grad} P_v)_{n+} - \frac{k}{\mu_w}(\operatorname{grad} P_w)_{n-} \quad (5)$$

$$\phi q \rho_w V_n + \frac{kq\rho_w}{\mu_w}(\operatorname{grad} P_v)_{n+} = \lambda_-(\operatorname{grad} T)_{n-} - \lambda_+(\operatorname{grad} T)_{n+} \quad (6)$$

Consider the action of capillary forces at the boiling front. Mechanical and thermodynamic equilibria at the interface require that the pressure gradient across the boiling front be defined by the relation

$$P_w = P_v + P_c \quad (7)$$

The capillary pressure value can be obtained from the Laplace formula

$$P_c = -2\frac{\sigma}{r}\cos\theta \quad (8)$$

where σ is the interfacial tension, θ the contact angle and r the mean radius of a capillary meniscus.

The influence of capillarity on phase transition at the interface is characterized by the Kelvin equation

$$P_v = P_f \exp(P_K), \quad P_K = -\frac{2\sigma V_m}{R_0\sqrt{k/\phi}} \quad (9)$$

where P_f is vapour pressure at the flat surface.

In order to obtain the mean capillary pressure, we use the well-known estimate for the typical length scale of a pore

$$d = \sqrt{\phi/k} \quad (10)$$

Since $r = d/2$, Eq. (8) for capillary pressure can be rewritten as

$$P_c = -4\sigma\sqrt{\frac{\phi}{k}}\cos\theta \quad (11)$$

For most real systems the contact angles cannot be measured accurately, with the result that some authors use capillary pressure values as input data for numerical simulations (see, for example, [2]).

We assume that all phases are in local thermodynamic equilibrium and the temperature on the interface ($x = X(t)$) is continuous; however the pressure jumps by the capillary pressure

$$P_{w*} - P_c = P_{v*}, \quad T_{w*} = T_{v*} \equiv T_* \quad (12)$$

In this case, the equation of the Clausius–Clapeyron curve may be written as

$$P_{v*} = P_a \exp\left[A - \frac{B + P_K}{T_*}\right]$$
$$A = 12.665, \quad B = -4697.28, \quad P_a = 10^5 \text{ Pa} \quad (13)$$

To solve the problem we apply the following boundary and initial conditions for the pressure and temperature

$$x = 0: \quad P_w = P^0, \quad T = T^0$$
$$t = 0: \quad P_v = P_0, \quad T = T_0 \quad (14)$$

2.3. Simplification of the basic equations

As the interface migrates slowly away from the injection well bore, the pressure distribution across the water zone is able to respond rapidly to changes in the front location, owing to the very small compressibility of water. Formally, this means that we can ignore the term on the left-hand side of Eq. (3). This term has an order $\delta P/t_{char}$, and the term on the right-hand side has an order $k\delta P/\phi\mu_w\alpha_w L_P^2$, where δP denotes the pressure variation, t_{char} is the characteristic time and L_P the characteristic length scale. The ratio of the right-hand side to the left-hand side is equal to dimensionless parameter

$$\epsilon = \frac{t_{char}}{L_P^2}\frac{k}{\phi\mu_w\alpha_w} \quad (15)$$

In order to estimate ϵ, we will use relation (5). As the first term on the right-hand side is negative, by ignoring the small ratio ρ_{v0}/ρ_w, we obtain

$$\phi V_n < -\frac{k}{\mu_w}(\operatorname{grad} P_w)_{n-} \quad (16)$$

From (16) we obtain an inequality for the characteristic values of the parameters

$$\frac{L_P^2}{t_{\text{char}}} < \frac{k\delta P_{\text{w}}}{\phi\mu_{\text{w}}} \quad \text{or} \quad 1 < \frac{t_{\text{char}}}{L_P^2}\frac{k\delta P_{\text{w}}}{\phi\mu_{\text{w}}} \tag{17}$$

Owing to the inequality $\delta P_{\text{w}} \gg 1/\alpha_{\text{w}}$, and using relation (17), we obtain

$$1 < \frac{t_{\text{char}}}{L_P^2}\frac{k\delta P_{\text{w}}}{\phi\mu_{\text{w}}} \ll \frac{t_{\text{char}}}{L_P^2}\frac{k}{\phi\mu_{\text{w}}\alpha_{\text{w}}} \tag{18}$$

If the dimensionless parameter ϵ is much larger than one then the time derivative on the left-hand side of Eq. (3) may be ignored; as a result we obtain a stationary equation for the pressure in the water region, $0 < x < X(t)$

$$\Delta P_{\text{w}} = 0 \tag{19}$$

or, for a one-dimensional system

$$\frac{\mathrm{d}^2 P_{\text{w}}}{\mathrm{d}x^2} = 0 \tag{20}$$

Eq. (19) was derived without special assumptions and this simplification allows to reduce the nonlinear energy equation (4) to a linear equation that describes advective and conductive heat transfer in the water region

$$(\rho C)_2\frac{\partial T}{\partial t} - \frac{k}{\mu_{\text{w}}}\rho_{\text{w}}C_{\text{w}}C_1\frac{\partial T}{\partial x} = \lambda_2\frac{\partial^2 T}{\partial x^2} \tag{21}$$

Here, C_1 is the constant of integration of Eq. (20).

As we are considering a relatively high-permeability reservoir with high injection rate, we can expect that temperature of the injected water ahead of the front has the same order as the initial reservoir temperature because the drop in temperature through the interface is controlled by the vaporization process only. Assuming that the difference between reservoir and vaporization pressure is small, the linear approach can therefore be applied to the vapour region [10]. As a result, we have a system of linear equations for the disturbances in the vapour region $X(t) < x < \infty$

$$\frac{\partial P'_{\text{v}}}{\partial t} = \kappa_1\frac{\partial^2 P'_{\text{v}}}{\partial x^2}, \quad \kappa_1 = \frac{kP_0}{\phi\mu_{\text{v}}} \tag{22}$$

$$\frac{\partial T'}{\partial t} = a_1\frac{\partial^2 T'}{\partial x^2}, \quad a_1 = \frac{\lambda_1}{(\rho C)_1} \tag{23}$$

where $P = P_0 + P'$, $T = T_0 + T'$.

3. Similarity solution

In order to illustrate the typical features of the influence of capillary pressure on water injection, we will consider the one-dimensional linear injection problem. We assume that the initial pressure P_0, injection pressure P^0, initial temperature T_0 and injection temperature T^0 are constants. The problem then admits a similarity solution

$$\begin{aligned} &P = P(\zeta), \quad T = T(\zeta), \\ &X(t) = 2\gamma\sqrt{a_2 t}, \quad \zeta = \frac{x}{2\sqrt{a_2 t}} \end{aligned} \tag{24}$$

In the vapour region $\gamma < \zeta < \infty$, the pressure and temperature distributions are given by

$$P_{\text{v}} = P_0 + (P_{\text{v}*} - P_0)\frac{\operatorname{erfc}(\zeta\sqrt{a_2/\kappa_1})}{\operatorname{erfc}(\gamma\sqrt{a_2/\kappa_1})} \tag{25}$$

$$T = T_0 + (T_* - T_0)\frac{\operatorname{erfc}(\zeta\sqrt{a_2/a_1})}{\operatorname{erfc}(\gamma\sqrt{a_2/a_1})} \tag{26}$$

where $\operatorname{erfc}(z)$ is the complementary error function.

In the water region $0 < \zeta < \gamma$, we obtain a linear distribution for the pressure

$$P_{\text{w}} = P^0 + (P_{\text{w}*} - P^0)\frac{\zeta}{\gamma} \tag{27}$$

An exact solution for the temperature has the form

$$\begin{aligned} T(\zeta) &= T^0 + (T_* - T^0)\frac{\operatorname{erfc}(\zeta + A) - \operatorname{erfc}(A)}{\operatorname{erfc}(\gamma + A) - \operatorname{erfc}(A)} \\ A &= \frac{k\rho_{\text{w}}C_{\text{w}}}{2\mu_{\text{w}}\lambda_2\gamma}(P_{\text{w}*} - P^0) \end{aligned} \tag{28}$$

By combining the above solutions with the boundary conditions (5), (6) and (13) we obtain two transcendental equations for the dimensionless unknown parameters γ and T_*

$$\begin{aligned} &\sqrt{\pi}\left(1 - \frac{\rho_{\text{v}*}}{\rho_{\text{w}}}\right)\gamma + \frac{\kappa_2}{a_2}\frac{\sqrt{\pi}}{2\gamma}\left(\frac{P_{\text{v}*}}{P_0} + \frac{P_{\text{c}}}{P_0} - \frac{P^0}{P_0}\right) \\ &\quad + \sqrt{\frac{\kappa_1}{a_2}}\left(\frac{P_{\text{v}*}}{P_0} - 1\right)\frac{\exp(-\gamma^2 a_2/\kappa_1)}{\operatorname{erfc}(\gamma\sqrt{a_2/\kappa_1})} = 0, \end{aligned} \tag{29}$$

$$\begin{aligned} &\frac{\sqrt{\pi}\phi\rho_{\text{w}}qa_2}{T_0}\gamma + \frac{\sqrt{\pi}}{2\gamma}\frac{kq\rho_{\text{w}}}{\mu_{\text{w}}T_0}(P_{\text{v}*} + P_{\text{c}} - P^0) \\ &\quad - \lambda_1\sqrt{\frac{a_2}{a_1}}\left(\frac{T_*}{T_0} - 1\right)\frac{\exp(-\gamma^2 a_2/a_1)}{\operatorname{erfc}(\gamma\sqrt{a_2/a_1})} \\ &\quad - \lambda_2\left(\frac{T_*}{T_0} - \frac{T^0}{T_0}\right)\frac{\exp(-\gamma^2)}{\operatorname{erfc}(\gamma)} = 0 \end{aligned} \tag{30}$$

$$P_{\text{v}*} = P_{\text{v}*}(T), \quad \rho_{\text{v}*} = \frac{P_{\text{v}*}}{\rho_{\text{w}}RT_*} \tag{31}$$

These equations are solved numerically for the typical values of the parameters.

3.1. Estimate of front velocity

Consider Eq. (29) at fixed initial reservoir temperature and pressure. If injection pressure P^0 increases then the similarity velocity of the liquid front γ will also increase. The first two terms in Eq. (29) increase with the injection pressure while the third term tends to a constant value and may be ignored. Thus, we obtain a simple estimate of the velocity of the liquid front as a function of parameters and the injection pressure

$$\gamma_{\text{est}} = \sqrt{\frac{\kappa_2}{2a_2}\left(1 - \frac{P_{\text{w}*}}{P^0}\right)} \equiv \sqrt{\frac{k(\rho C)_2}{2\lambda_2\phi\mu_{\text{w}}}(P^0 - P_{\text{w}*})} \tag{32}$$

It should be noted that as the third term in (29) describes the vapour flux, the estimate corresponds to a piston-displacement regime of water injection.

If we consider the vapour flux ahead of the front, the estimate can be corrected using the smallness of the parameter $\gamma^2 a_2/\kappa_1$ and the first term of the expansions into series of the complementary error function and exponent function. An estimate of the parameter $\gamma\sqrt{\frac{a_2}{\kappa_1}}$ gives a value of about 0.27. As mentioned above, the deviation of the vaporization temperature from the reservoir temperature is small, with the result that we can use approximatively $P_{v*} \approx P_f(T_0)$ and $\rho_* \approx P_f(T_0)/RT_0$. Consequently, we obtain a quadratic equation for the parameter γ

$$\gamma_{est}^2 + S_1\gamma_{est} + S_2 = 0,$$
$$S_1 = \sqrt{\frac{\kappa_1}{\pi a_2}}\frac{\rho_v}{\rho_w}\left(\frac{P_{v*}}{P_0} - 1\right), \quad S_2 = \frac{\kappa_2}{2a_2}\left(\frac{P_{w*}}{P^0} - 1\right) \tag{33}$$

The equation has two roots but the positive one only has a physical meaning

$$\gamma_{est} = -\frac{S_1}{2} + \sqrt{\frac{S_1^2}{4} - S_2} \tag{34}$$

These estimates show that for a relatively high-permeability reservoir and a large flow rate the effect of heat redistribution on the process is small and the process is close to a piston-displacement regime.

4. Comparison of analytical solution and numerical simulations

Numerical experiments were performed for typical values of the system parameters shown in Table 1 to compare numerical results and estimates from the simplified analytical model, using the multiphase fluid and heat flow simulator TOUGH2 [6]. We considered a 1-D homogeneous porous medium column with a relatively fine grid near the injection point (500 elements with grid spacing of 1 m) to resolve the sharp thermal and phase fronts there. For $x > 500$ m grid spacing was increased out to a total length of 100 km (system infinite acting for the periods of time simulated). Cross sectional area is 1 m^2. The system is initially saturated with superheated vapour at a uniform temperature of 550 K and pressure in the range 0.5–5 MPa. Cold (300 K) water injection at one end of the column is represented by a boundary element at constant temperature and pressure. Initial reservoir conditions are maintained constant at the other end of the system by another boundary element.

Fig. 1 shows a typical distribution of the temperature as a function of the similarity variable for a regime of high injection rate. The vaporization process at the moving front causes a decrease in phase transition temperature owing to heat absorption. A small "boundary" layer near the injection well is characterized by the value of the rock heat conductivity coefficient. On the whole, Fig. 1 identifies an excellent agreement between the analytical results and numerical simulations.

Table 1
Parameters used in numerical simulations

Formation parameters		
Rock density	2600	kg/m^3
Porosity	.10	
Thermal conductivity	2.51	W/m K
Specific heat of rock	920	J/kg K
Permeability	10^{-15}–10^{-16}	m^2
Relative permeability		
van Genuchten-Mualem model	$\lambda = .4438$, $S_{lr} = .081$, $S_{ls} = 1$, $S_{gr} = .01$	
Capillary pressure		
van Genuchten function	$m = .4438$, $S_{lr} = .0801$, $S_{ls} = 1$	
	$1/P_0 = 5.79 \times 10^{-7}$	Pa^{-1}
	$P_{max} = 7.52$–23.77×10^5	Pa
Reservoir initial conditions		
Temperature	550	K
Pressure	2	MPa
Injection specifications		
Temperature	300	K
Pressure	8–14	MPa

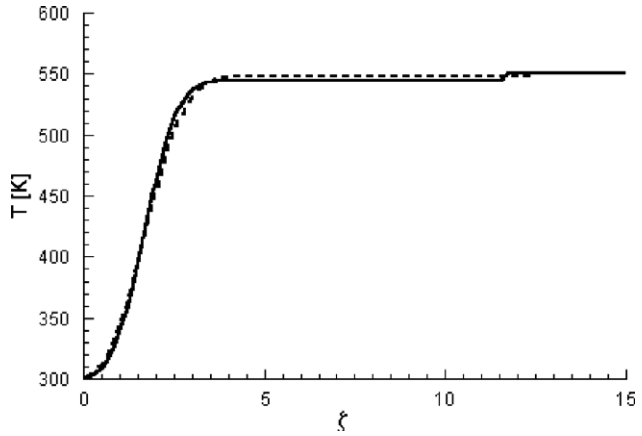

Fig. 1. Typical temperature distribution as a function of similarity variable for water injected into superheated wettable rock. Solid line – analytical solution, dashed line – numerical result. $\theta = 15°$ ($P_c = -7.52 \times 10^5$ Pa), $T_0 = 550$ K, $T^0 = 300$ K, $k = 10^{-15}$ m^2, $P_0 = 2 \times 10^6$ Pa, $P^0 = 10^7$ Pa.

Fig. 2 illustrates the typical pressure distributions for neutral, wettable, and nonwettable rock. In the first case the pressure is a continuous function, whereas in the other two cases it has discontinuities. As capillary pressure P_c is negative for the wettable rock, the pressure at the boiling front is smaller than the vapour pressure ahead of the front. For the nonwettable rock, when capillary pressure is positive, the water pressure at the front is larger than the vapour pressure. An increase in the water pressure at the front decreases pressure gradient in the liquid region and, respectively, water flux, so that the amount of injected

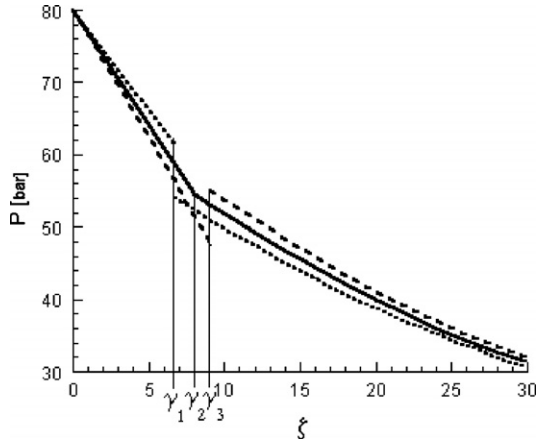

Fig. 2. Pressure distributions for three different contact angles. Results obtained from analytical solutions. Solid, dashed and dotted lines denote neutral, wettable and nonwettable media $\theta = 90°, 15°, 165°$, respectively. Other parameters as in Fig. 1.

water is larger for the wettable medium. In the case the capillary pressure plays the role of a suction pressure.

Fig. 3 compares the analytical and numerical results for the wettable rock. It is seen that the pressure gradient calculated numerically has a band near the injection well that corresponds to the narrow region in which temperature and viscosity vary considerably. The pressure gradient is therefore larger in this domain, which is characterized by large viscosity values. The pressure gradient near the well, calculated from the analytical solution, is smaller than the gradient obtained from numerical calculations, but is larger behind the front, as the analytical solution uses the arithmetic mean value for the water viscosity. For the wettable rock, the frontal analytical solution shows that the pressure behind the interface falls below saturation pressure, that indicates superheating of the water. In this case, an extended water-vapour phase transition zone forms between the water and vapour regions as showing numerical simulations. This zone corresponds to the horizontal part of the dashed line of the pressure distribution. As seen here, the position of the sharp front obtained from analytical solution practically coincides with the middle of the two-phase zone.

The different calculated values of γ for a wettable rock are presented in Fig. 4, which shows that the front velocity, as quantified by γ, increases with the injection pressure. Comparison of both asymptotic estimates (dashed and dotted lines) with the numerical simulation results shows a very good agreement between the two. Some differences may occur between the exact solution and numerical results because of the comparatively rough estimate of the main parameters used as functions of the arithmetic mean of the temperature values in the analytical approach.

Fig. 5 presents the interface velocity, which is calculated analytically for nonwettable, neutral and wettable media.

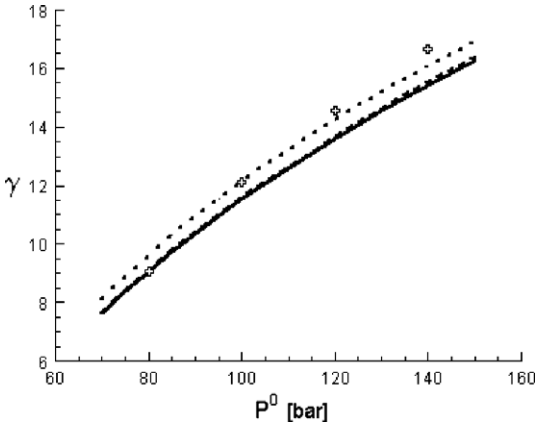

Fig. 4. Variation of the liquid front as a function of injection pressure. The solid line represents the exact analytical result; dashed line marks the results obtained from relation (34); the dotted line shows the simplest estimate (relation (32)) and the crosses mark the results of numerical calculations. Profiles are shown for the same data as in Fig. 1.

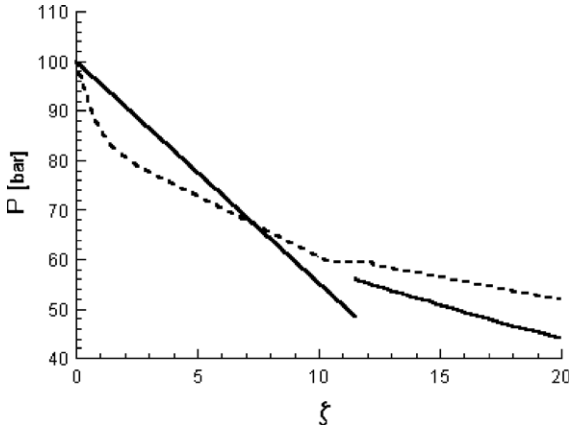

Fig. 3. Comparison of pressure distribution from analytical solution (solid line) and numerical simulations (dashed line). Profiles are shown for the same data as in Fig. 1.

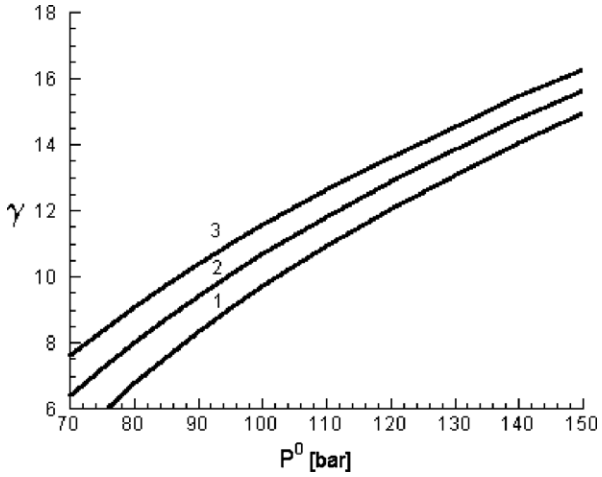

Fig. 5. Interface velocity versus reservoir pressure for nonwettable (curve 1, $\theta = 165°$), neutral (curve 2, $\theta = 90°$) and wettable (curve 3, $\theta = 15°$) media. Profiles are shown for the same data as in Fig. 1.

The velocity is seen to increase when the contact angle decreases.

Fig. 6 illustrates how the speed of the liquid front varies with rock permeability for other given parameters. The figure indicates that, in wettable media, the liquid front always moves more rapidly.

When rock permeability decreases to $k = 10^{-16}\,\mathrm{m}^2$ (Fig. 7) then, as it follows from relation (11), the capillary pressure increases and, in the case of nonwettable media, for $\theta = 165°$, we obtain that $P_c = 2.3 \times 10^6$ Pa. For the wettable rock, when $\theta = 15°$, $P_c = -2.3 \times 10^6$ Pa. Fig. 7 shows that, for a small injection rate (small injection pressure P^0), the speed of the liquid front depends mainly on capillary pressure. As numerical calculations show, the extended vaporization region is formed and in this case the analytical solution provides a rough estimate of the parameters.

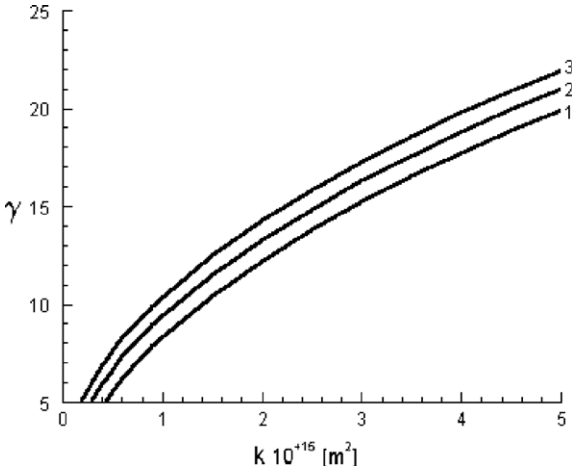

Fig. 6. Interface velocity versus rock permeability for nonwettable (curve 1, $\theta = 165°$), neutral (curve 2, $\theta = 90°$) and wettable (curve 3, $\theta = 15°$) media. Profiles are shown for the same data as in Fig. 1.

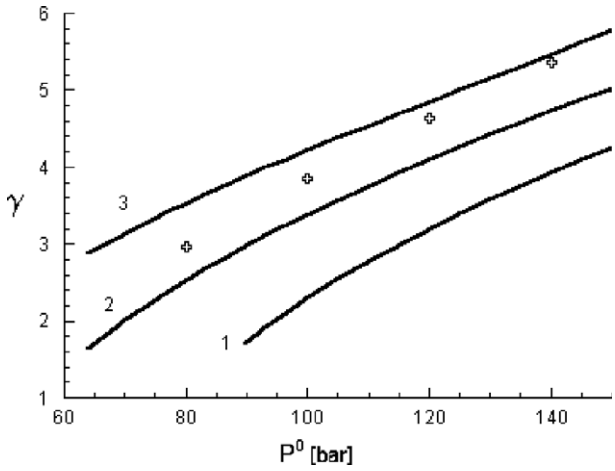

Fig. 7. Interface velocity versus reservoir pressure for nonwettable (curve 1, $\theta = 165°$), neutral (curve 2, $\theta = 90°$) and wettable (curve 3, $\theta = 15°$) media. Open crosses mark the results of numerical calculations. Low-permeability media $k = 10^{-16}\,\mathrm{m}^2$. Other parameters as in Fig. 1.

5. Conclusions

A simplified mathematical model of cold water injection into hot permeable rock which includes the capillary pressure effects was developed. An analytical solution was derived and compared with the numerical simulations carried out by TOUGH2 code [6]. Our analysis has established that the predictions from the analytical solution are in agreement with the numerical results and allow to obtain a good estimate for the liquid front velocity.

We identified that the injection rate increases with the capillary forces for a wettable rock and decreases for a nonwettable media. Our results for the fixed porosity $\phi = 0.1$ indicate that cold water injection into the hot rock depends on capillary pressure if rock permeability is less than $10^{-15}\,\mathrm{m}^2$. For a small injection rate the velocity of the liquid front is determined mainly by the capillary pressure. Capillary forces in wettable media causes a formation of an extended water-vapour phase transition zone which separates the single-phase regions. It is shown in Fig. 7 that for the low-permeability wettable rock the analytical approach has good applicability for the high injection pressure because the injection pressure reduces the extension of the two-phase zone. If the water-vapour transition zone is small then the analytical approach provides an adequate result as uses the sharp front approximation. This result is in contrast to the case with the relatively high permeability and small injection pressure (Fig. 4) when the similarity solution is in good agreement with the numerical result; whereas, there is a large difference between the analytical and numerical results for high injection rate.

As it may be seen in Fig. 1 for the large injection pressure the extended plateau of high temperature and low viscosity is formed. The decrease in the water viscosity leads to the increase in the liquid flux and front velocity. This circumstance cannot be accounted for in the analytical solution, because the water viscosity is determined as the mean arithmetic of the injection and reservoir pressure. Therefore, the difference between the results of the two methods for a large injection pressure may be caused by a rough estimate of the water viscosity in the analytical solution.

Comparison of the similarity and numerical approaches provides a more effective way to full understanding of the effect of capillary forces on injection rate and boiling regime, and also identify the parameters at which simple estimates from analytical solution can be applied.

Acknowledgement

This work was supported by NATO grant EST.NR.EV 980623 and the Short Term Mobility Program of CNR.

References

[1] K.S. Udell, Heat transfer in porous media: considering phase change and capillarity – the heat pipe effect, Int. J. Heat Mass Transfer 28 (1985) 485–495.

[2] K. Pruess, M. O'Sullivan, Effect of capillarity and vapor adsorbtion in the depletion of vapor-dominated geothermal reservoirs, in: Proceedings, XVIIth Workshop on Geothermal Reservoir Engineering, Stanford, California, January 29–31, 1992, pp. 165–174.

[3] K. Pruess, Numerical simulation of water injection into vapor-dominated reservoirs, Proceedings World Geothermal Congress, Florence, Italy, vol. 3, 1995, pp. 1673–1679.

[4] K. Li, R.N. Horne, An experimental and analytical study of steam/water capillary pressure, SPE Reservoir Evaluation Eng. 4 (2001) 477–482.

[5] K. Li, R.N. Horne, Steam/water capillary pressure, in: Proceedings World Geothermal Congress, Antalya, Turkey, Paper N 1151, 2005.

[6] K. Pruess, C. Oldenburg, G. Moridis, TOUGH2 User's Guide, Version 2.0, Lawrence Berkeley National Laboratory Report LBNL 43134, 1999.

[7] K. Pruess, C. Calore, R. Celati, Y.S. Wu, An analytical solution for heat transfer at a boiling front moving through a porous medium, Int. J. Heat Mass Transfer 30 (1987) 2595–2602.

[8] S.K. Garg, J.W. Pritchett, Pressure interference data analysis for two-phase (water/steam) geothermal reservoirs, Water Resour. Res. 24 (1988) 843–852.

[9] A.W. Woods, S.D. Fitzgerald, The vaporization of a liquid front moving through a hot porous rock, J. Fluid Mech. 251 (1993) 563–579.

[10] A.A. Barmin, G.G. Tsypkin, On motion phase transition front at water injection into vapour-saturated geothermal reservoir, Sov. Phys. Dokl. 41 (1996) 315–320.

[11] A.W. Woods, Liquid and vapour flow in superheated rock, Ann. Rev. Fluid Mech. 31 (1999) 171–199.

[12] G.G. Tsypkin, A.W. Woods, Vapour extraction from a water saturated geothermal reservoir, J. Fluid Mech. 506 (2004) 315–330.

[13] G.G. Tsypkin, C. Calore, A mathematical model for water-vapour phase transitions in geothermal system with allowance for capillary pressure, Phys. Dokl. 47 (2002) 495–498.

[14] G.G. Tsypkin, C. Calore, Role of capillary forces in vapour extraction from low-permeability, water-saturated geothermal reservoir, Geothermics 32 (2003) 219–237.

[15] D.H. Brownell, S.K. Garg, J.W. Pritchett, Governing equations for geothermal reservoirs, Water Resour. Res. 13 (1977) 929–934.

[16] C.R. Faust, J.W. Mercer, Geothermal reservoir simulation. 1. Mathematical models for liquid- and vapor-dominated hydrothermal systems, Water Resour. Res. 15 (1979) 23–30.